

This is the accepted manuscript made available via CHORUS. The article has been published as:

# Spontaneous forward Brillouin scattering in carbon disulfide

Ryan O. Behunin, Yi-Hsin Ou, and Khanh Kieu

Phys. Rev. A **99**, 063826 — Published 20 June 2019

DOI: [10.1103/PhysRevA.99.063826](https://doi.org/10.1103/PhysRevA.99.063826)

# Spontaneous forward Brillouin scattering in carbon disulfide

Ryan O. Behunin

*Department of Physics and Astronomy, Northern Arizona University, Flagstaff, AZ 86011*

Yi-Hsin Ou and Khanh Kieu

*College of Optical Sciences, University of Arizona, Tucson, AZ 85721 USA.*

(Dated: May 14, 2019)

In recent years, guided acoustic wave Brillouin scattering has become an important tool in photonics, serving as the basis for everything from new forms of information processing to silicon lasers. Due to low losses and long interaction lengths, fiber optic systems offer an intriguing platform to harness these guided-wave light-sound interactions. However, within typical fiber optic systems these interactions are exceedingly weak—requiring complex microstructuring to yield appreciable light-sound coupling. Here, we enhance this light-sound coupling by using a CS<sub>2</sub>-filled liquid core optical fiber. Owing to tight confinement of the optical and acoustic modes within the fiber core, as well as the large electrostrictive response of CS<sub>2</sub>, this system yields an unprecedented forward Brillouin gain for a fiber optic system. To demonstrate this physics, we measure multi-peaked spontaneous forward Brillouin scattering power spectra, yielding information about the fiber geometry, material properties, and acousto-optic coupling strength. To interpret these data, we simulate the spontaneous Brillouin scattering power spectrum for this fiber system. These results reveal that hybridized acoustic excitations within the fiber core and cladding produce this characteristic multi-peaked power spectrum. In the future, the large forward Brillouin coupling, long interaction lengths, and low losses of liquid-core fibers may enable new forms of distributed sensing, lasers with customizable emission, and physics including continuum optomechanical cooling.

## I. INTRODUCTION

The advent of photonic crystal fibers (PCF) and optomechanical waveguides on silicon chips has instigated a surge of interest in guided acoustic wave Brillouin scattering [1–5]. Within these systems, tight confinement of light and sound to nanoscale waveguides can produce large tailorable acousto-optic interactions that have enabled new forms of information processing [6, 7], optical amplification [8–10], laser dynamics [11], and laser cooling of traveling wave phonons [12]. The long interaction lengths and low losses of optical fiber systems make them an intriguing platform in which to harness these interactions. However, due to weak acoustic confinement, guided wave Brillouin interactions are weak within standard optical fibers [13, 14].

Similar to advances in Brillouin physics made possible by photonic crystal fibers [1–3], liquid-core optical fibers (LCOF) offer an intriguing opportunity to harness guided acoustic wave Brillouin coupling [15]. LCOFs can support low-loss single mode operation, can be integrated with standard optical fibers, and can produce large Brillouin couplings [16]. The strength of light-sound (Brillouin) coupling within a waveguide is controlled by the overlap of the optical and acoustic fields and by the magnitude of electrostrictive coupling [17]. By utilizing high-index liquids these fibers can produce highly confined optical modes [15], and given the large mechanical impedance mismatch between most liquids and solids, acoustic excitations can be tightly trapped within the core [18, 19]. Combining the massive electrostrictive couplings produced in high-index liquids with tight acousto-optic overlap, it may be possible to produce large guided

acoustic wave Brillouin couplings within LCOFs.

In this paper, we utilize a LCOF system to demonstrate spontaneous forward Brillouin scattering in CS<sub>2</sub> for the first time. Using heterodyne spectroscopy, we measure spontaneous forward Brillouin scattering spectra, revealing the frequency and linewidth of the participating phonons and the magnitude of the Brillouin coupling. We model this physics using the theory of spontaneous guided acoustic wave scattering in combination with finite element simulations to yield complex Brillouin spectra showing good agreement with measurements [18, 20]. These simulations show that this CS<sub>2</sub>-filled LCOF system supports single-mode operation of a tightly confined optical mode with a 1550 nm wavelength, as well as a family of cut-off guided acoustic waves. As a result of the tight overlap of these optical and acoustic modes (produced by the small 0.9  $\mu\text{m}$  core radius) and the large electrostrictive response of CS<sub>2</sub>, we measure an unprecedented forward Brillouin gain coefficient  $\sim 5.8 \text{ (Wm)}^{-1}$  for a fiber optic system—a guided-wave acousto-optic coupling more than three times larger than those reported in photonic crystal fibers and nearly 3 orders of magnitude larger than the  $\sim 8 \times 10^{-3} \text{ (Wm)}^{-1}$  estimated forward Brillouin gain coefficient for standard single-mode optical fiber (SMF-28) [3].

The paper is organized as follows: In Sec. I, we discuss the phenomenology of spontaneous forward Brillouin scattering. Section II describes the LCOF optical fiber sample and measurement technique. Section III compares the spontaneous forward Brillouin scattering data with measurements and interprets the spectra.

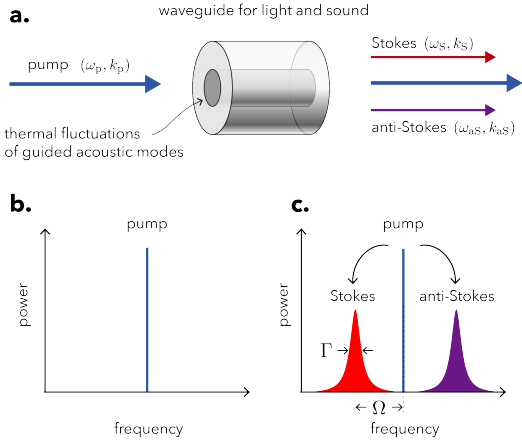


FIG. 1. (a) Phenomenology of spontaneous forward Brillouin scattering. (b) A laser scatters from thermally populated guided acoustic waves, (c) producing Stokes and anti-Stokes sidebands.

## II. SPONTANEOUS FORWARD BRILLOUIN SCATTERING

Spontaneous forward Brillouin scattering (SFBS) occurs when light scatters from thermally excited guided phonons within a transparent material, leading to new frequencies of copropagating photons (see Fig. 1). The efficiency of this scattering process is maximized when phase matching between all participating waves is satisfied. For example, for the Stokes process (see Fig. 1c), an incident pump photon of frequency  $\omega_p$  is red-shifted to a lower frequency Stokes photon of frequency  $\omega_s$  by scattering from a phonon. When this process occurs within a waveguide for light and sound, phase matching requires  $\omega_p = \omega_s + \Omega$ , where  $\Omega$  is the angular frequency of the phonon, and  $k_p = k_s + q$  (Fig. 2), where  $k_p$ ,  $k_s$  and  $q$  are the respective wavevectors of the copropagating pump, Stokes, and phonon modes. By using the dispersion relation for the optical fields, i.e.  $\omega = (c/n)k$  where  $n$  is the effective refractive index, and assuming that  $n$  takes the same value for the pump and Stokes modes, these phase matching conditions require  $\Omega = (c/n)q$ , or in other words, the phase velocity of phonons mediating forward Brillouin scattering is the same as light. In an acoustic waveguide, this condition can be satisfied by cut-off acoustic modes (see Fig. 2).

The interaction between light and sound required for Brillouin scattering is enabled by electrostriction [21], a process where elastic strain can be induced within a transparent medium by the presence of electromagnetic energy. Radiation pressure can also play a critical role in Brillouin coupling for waveguides with sub-wavelength dimensions [22]. In the LCOF system described here, however, radiation pressure is negligible, contributing less than 0.001 % of the Brillouin coupling produced by electrostriction.

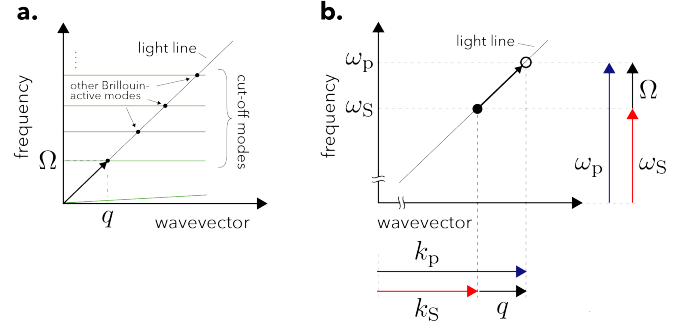


FIG. 2. Phase matching conditions for forward Brillouin scattering. (a) Dispersion relations (green) for a collection of guided-acoustic waves near  $q = 0$ , the intersection of the depicted light line with each dispersion curve gives the frequency and wavevector for each Brillouin-active acoustic mode. (b) Dispersion relation for light. The frequency and wavevector of a forward Brillouin-active phonon mode can couple two distinct (pump & Stokes) optical modes.

Spontaneous forward Brillouin scattering reveals a wealth of information about guided acoustic modes within a waveguide. The scattered light is spaced from the pump by a frequency  $\Omega/(2\pi)$  and spread over a bandwidth  $\Gamma/(2\pi)$ , determined by the phonon resonance frequency and decay rate respectively. In sharp contrast with backward Brillouin scattering, the phase-matched phonon frequencies in SFBS are determined by the waveguide geometry [14, 18, 19] and are, to an excellent approximation, independent of the pump wavelength and given by the cut-off frequency of the guided acoustic modes. Consequently, spontaneous forward Brillouin scattering spectra enable a unique form of phonon spectroscopy, yielding information about the waveguide geometry, composition, and acoustic dissipation.

## III. EXPERIMENT DESCRIPTION & RESULTS

We explore spontaneous forward Brillouin scattering in a **0.95 meter long** CS<sub>2</sub>-filled silica capillary of inner radius 0.9  $\mu\text{m}$  and outer radius  $\sim 64.5\mu\text{m}$  (see Fig. 3) [15]. **To couple light into the LCOF, we fusion splice an angle-cleaved high numerical aperture fiber (Nufern UHNA7) to the capillary. The angle cleave leaves a small gap where liquid can enter the center of the capillary, and a sealed vial surrounding the splice contains the liquid CS<sub>2</sub> (see Ref. [15] for more details on the LCOF). It is imperfect coupling of light through these splices that dominate the optical losses, yielding  $\sim 22\%$  transmission through the sample used in this paper.**

Due to the large electromagnetic and acoustic impedance mismatch between CS<sub>2</sub> and silica, this system supports a single guided electromagnetic mode at a wavelength of  $1.55\mu\text{m}$  (Fig. 3c) and a family of guided acoustic modes that are tightly confined to the core (Figs.

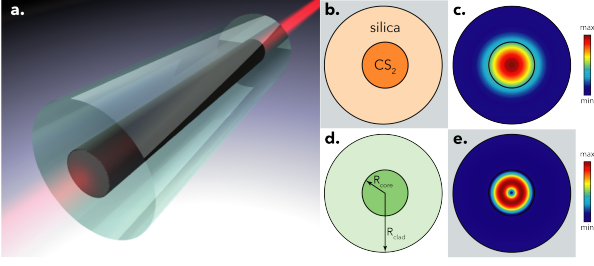


FIG. 3. (a) Illustration of LCOF system. Cross-section of liquid-core fiber system (not to scale) showing (b) layout of materials, (c) electric field norm for a guided electromagnetic mode, (d) labels for the geometry  $R_{\text{core}} = 0.9 \mu\text{m}$  and  $R_{\text{clad}} \approx 64.5 \mu\text{m}$ , and (e) one example of an acoustic mode that is tightly trapped within the core.

2a & 3e). This tight overlap of these guided modes within the core, in combination with the large electrostrictive response of  $\text{CS}_2$  [21], is critical to produce the large Brillouin coupling of this system.

We measure spontaneous forward Brillouin scattering in  $\text{CS}_2$ -filled LCOF using the apparatus shown in Fig. 4. After being amplified, a pump laser is sent through the liquid-core fiber (see Fig. 4a). Thermal fluctuations of the phonon modes within the fiber produce a phase-modulation of the incident pump light producing Stokes and anti-Stokes sidebands (Fig. 4b) that encode information about the Brillouin active phonon modes. For the purpose of heterodyne detection, we remove the anti-Stokes sideband, which is comparable in magnitude to the Stokes sideband, by passing the scattered light through a band-pass filter (Fig. 4c). **This filter is created using a tunable fiber Bragg grating with a 5 GHz reflection bandwidth and a sharp roll-off. By placing the pump laser at the short wavelength edge of the reflection band, we reduce transmission of the scattered anti-Stokes light by  $\sim 30$  dB.** After filtering, we photomix the transmitted and scattered pump light on a high-speed receiver. The transmitted pump laser acts as a local oscillator, interfering with the scattered Stokes light to produce a radio-frequency beatnote that is measured on a spectrum analyzer, yielding spectra of the type shown in Figs. 5 & 6. It is important to note that without the filtering step described above, the anti-Stokes sideband can produce a radio-frequency photocurrent that destructively interferes with the Stokes-pump beatnote, effectively cancelling the Brillouin scattering signal.

#### IV. ANALYSIS

To interpret these data, we utilize the theory of spontaneous forward Brillouin scattering, models of Brillouin coupling in step-index waveguides, and finite-element simulations of the acoustic and optical modes of the LCOF [17, 20]. Using these results, we can calculate the

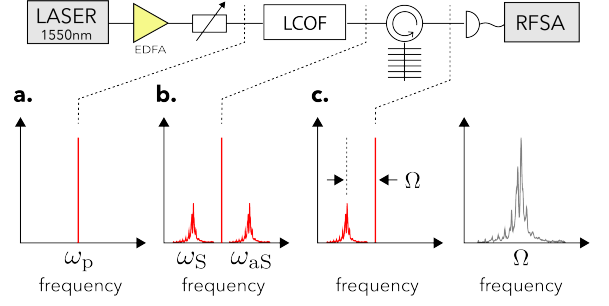


FIG. 4. Apparatus for heterodyne spectroscopy of spontaneous forward Brillouin scattering. A pump laser, amplified by an erbium-doped fiber amplifier (EDFA), is passed through the liquid-core fiber and filtered. The filtered output of the LCOF, comprising the transmitted pump (local oscillator) and scattered light, is photomixed and detected on a radio-frequency spectrum analyzer (RFSA).

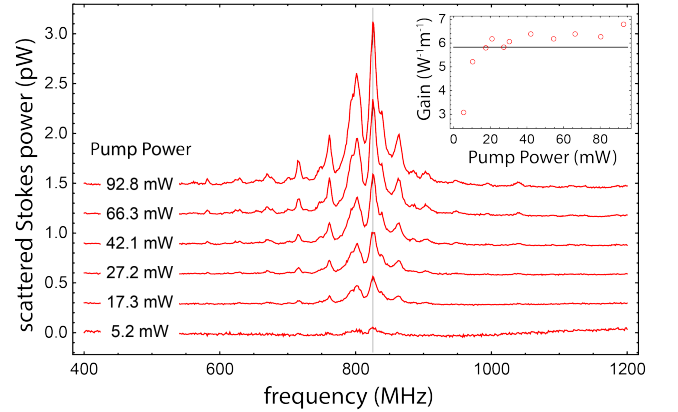


FIG. 5. Spontaneous forward Brillouin Stokes power spectra versus intra-fiber pump power. Power spectra are offset 0.3 pW with increasing power for clarity. Inset: Estimated Brillouin gain obtained for peak located at 827 MHz (see vertical line). Horizontal line is given by best fit to data, yielding  $G_B = 5.8 \pm 1 (\text{Wm})^{-1}$ .

power spectrum of spontaneously scattered Stokes light given by

$$S(\omega) = \sum_j \frac{G_{B,j}(n_{\text{th},j} + 1)\Gamma_j^2/4}{(\omega - \Omega_j)^2 + \Gamma_j^2/4} LP_p, \quad (1)$$

where  $P_p$  is the injected pump power,  $L$  is the waveguide length, and  $j$  labels the Brillouin gain  $G_{B,j}$ , thermal occupation number  $n_{\text{th},j}$ , angular frequency  $\Omega_j$  and decay rate  $\Gamma_j$  for the  $j$ th Brillouin-active acoustic mode [20]. Here, the thermal occupation number is defined by  $n_{\text{th},j} \equiv (\exp\{k_B T / \hbar \Omega_j\} - 1)^{-1}$  where  $k_B$ ,  $T$ , and  $\hbar$  are Boltzmann's constant, the temperature, and Planck's constant. We obtain these acoustic mode specific parameters through finite element simulations that account for the detailed LCOF geometry and material properties. These simulations incorporate empirically ob-

tained indices of refraction, density, and elastic moduli for CS<sub>2</sub>, fused silica and the polyimide buffer, the frequency dependent acoustic dissipation in silica and CS<sub>2</sub> [23, 24], and the effects of the polyimide coating on acoustic mode shape, frequency, and dissipation. Through these calculations, we obtain the complex eigenfrequencies  $\Omega_j + i\Gamma_j/2$  and the profiles for the LCOF's optical and acoustic modes. Combining these results, we quantify the Brillouin gain  $G_{B,j}$  for each guided acoustic wave (see Appendix A).

In Fig. 6, we compare normalized measurements of spontaneous forward Brillouin scattering to the predicted spectra. These simulations accurately capture the critical features of the measured power spectra, reproducing the center frequency and relative heights of the various Brillouin resonances.

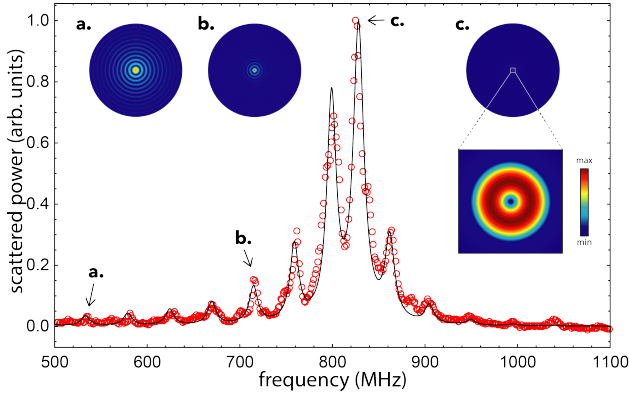


FIG. 6. Spontaneous forward Brillouin scattering spectrum. Open red circles are measurements and solid line is simulated spectrum. Both measured and simulated spectra have been normalized to peak gain. For this comparison, a small contribution from the scattered power background is subtracted and the resulting power spectrum is scaled to have a max value of unity. The insets (a), (b) and (c), show the magnitude of the acoustic displacement along fiber cross-section—illustrating that the spectra subpeaks (e.g. see (a)) represent motion spanning the fiber cladding and that the large peaks near 800 MHz (see points (b) and (c)) comprise acoustic motion that is tightly trapped within the fiber core.

Through these results, we obtain important information about this fiber system. We identify a collection of acoustic modes, hybridized between the core and cladding, as the source of the various peaks observed in the spectrum. Acoustic modes trapped tightly within the core produce the large peaks near 800 MHz, and are sensitive to the core geometry (see inset and point c of Fig. 6). Whereas, the smaller peaks, e.g. point a of Fig. 6, comprise elastic motion distributed over the fiber cross-section, with relative spacing highly dependent on the cladding diameter. Hybridized elastic motion between the core and the cladding produce the resonances of intermediate gain, e.g. point b of Fig. 6. In particular, we can use the frequencies of the small peaks to estimate the cladding diameter of  $\sim 129\mu\text{m}$ , in agreement with

independent measurements of the fiber geometry.

We estimate the Brillouin gain from the scattered Stokes power at the peak of the power spectrum  $P_{S,\text{peak}}$  (see Fig. 5). By integrating Eq. 1 over the (10 kHz) resolution bandwidth of the spectrum analyzer ( $\Delta\nu$ ) centered on the peak ( $\omega = \Omega_{\text{peak}} = (2\pi)827\text{ MHz}$ ) of the measured power spectrum, we obtain the following expression for Brillouin gain given in terms of  $P_{S,\text{peak}}$

$$G_{B,\text{peak}} \approx \frac{\Omega_{\text{peak}}}{\Delta\nu k_B T \omega_p L P_p} P_{S,\text{peak}} \quad (2)$$

where we have used  $k_B T \gg \hbar\Omega_{\text{peak}}$  (valid for this system) to approximate the thermal occupation as  $n_{th} \approx k_B T / \hbar\Omega_{\text{peak}}$ . We plot  $G_{B,\text{peak}}$  in the inset of Fig. 5, showing an estimated forward Brillouin gain of  $5.8 \pm 1 (\text{Wm})^{-1}$ . Our simulations predict a peak gain of  $G_B = 15.8 (\text{Wm})^{-1}$ —a discrepancy we attribute to imperfect coupling of light into the fiber, uncertainties in intra-fiber and transmitted powers and the optical-to-radio frequency calibration. With reported guided acoustic wave Brillouin gain coefficients of  $2.5 \times 10^{-2} (\text{Wm})^{-1}$  in FSV 6000Å [13, 14],  $1.7 \times 10^{-2} (\text{Wm})^{-1}$  in highly-nonlinear fiber [25], and  $1.5 (\text{Wm})^{-1}$  in PCF [3], to our knowledge this CS<sub>2</sub>-filled LCOF produces the largest guided-acoustic wave Brillouin coupling reported in a fiber optic system to date. Moreover, our simulations reveal a path to even larger acousto-optic couplings, predicting a peak forward Brillouin gain of order  $\sim 50 (\text{Wm})^{-1}$  if the polyimide buffer is removed, a prediction similar to observations in standard optical fibers [14].

*Conclusion:* In this paper, we demonstrated forward Brillouin scattering in CS<sub>2</sub> for the first time. Using optical heterodyne spectroscopy, we measured complex multi-peaked power spectra of spontaneously scattered Stokes light, yielding an unprecedented forward Brillouin gain coefficient of  $\sim 5.8 (\text{Wm})^{-1}$  in an optical fiber. This large Brillouin gain is made possible by the unique features of CS<sub>2</sub>-filled LCOFs, which tightly confine light and sound to the  $0.9\mu\text{m}$  radius fiber core where the large photoelastic constant of CS<sub>2</sub> can efficiently produce acousto-optic coupling. Finite-element simulations of the acousto-optic physics reproduce the critical features of our measurements, revealing that the multi-peaked nature of these power spectra arises from a family of hybridized acoustic excitations between the fiber core and cladding.

In the future, the large forward Brillouin gain achievable in this LCOF system, coupled with the long interaction lengths afforded by fiber optics, may open the door to new fiber-based applications based on forward Brillouin scattering. For example, the Brillouin spectrum sensitivity to the fiber geometry, material properties, and the acoustic dissipation may enable new forms of distributed sensing [1, 26, 27]. By leveraging the unique properties of forward Brillouin scattering, this large gain can be harnessed to create everything from optical amplifiers with engineered gain properties [8, 9], to new forms



of all-optical signal processing [6, 7].

### ACKNOWLEDGMENTS

R.B. acknowledges support through NAU start-up funds, valuable discussions with Nils Otterstrom and Peter Rakich, and experimental assistance from Megan Chambellan. K.K. acknowledges support from the Air Force Office of Scientific Research (AFOSR, FA9550-15-1-0389) and fruitful suggestions of Dr. Gernot Pomrenke.

### Appendix A: Brillouin gain calculation

We calculate the Brillouin gain spectrum by utilizing finite element simulations of the optical and acoustic modes of the LCOF. By including empirically derived material properties (see Tab. I) and damping for silica [24] and CS<sub>2</sub> [23], these simulations yield the acoustic mode eigenfrequencies  $\Omega_j$  and dissipation rates  $\Gamma_j$  as well as the spatial mode profiles for the electric field  $\mathbf{E}$  and the elastic displacement  $\mathbf{u}_j$ . We obtain the Brillouin gain by evaluating the spatial overlap of these modes given by the formula

$$G_{B,j} = \frac{2\omega_p}{\Omega_j \Gamma_j v_g^2} \frac{|\langle \mathbf{f}, \mathbf{u}_j \rangle|^2}{\langle \mathbf{E}, \varepsilon \mathbf{E} \rangle^2 \langle \mathbf{u}_j, \rho \mathbf{u}_j \rangle} \quad (\text{A1})$$

where  $v_g$  is the optical group velocity,  $\varepsilon$  and  $\rho$  are the spatially dependent dielectric permittivity and mass density, respectively, and  $\langle \mathbf{A}, \mathbf{B} \rangle \equiv \int_{wg} d^2x \mathbf{A}^* \cdot \mathbf{B}$  with  $wg$  denoting an integration over the waveguide cross-section. For propagation along the z-axis, the electrostrictive force density  $\mathbf{f}$  is given by

$$f_x = -\frac{1}{2} \varepsilon_0 n^4 \partial_x (p_{11} |E_x|^2 + p_{12} (|E_y|^2 + |E_z|^2) + 2p_{44} \text{Re}[E_x E_y^*]) \quad (\text{silica}) \quad (\text{A2})$$

$$f_y = -\frac{1}{2} \varepsilon_0 n^4 \partial_y (p_{12} |E_x|^2 + p_{11} (|E_y|^2 + |E_z|^2) + 2p_{44} \text{Re}[E_x E_y^*]) \quad (\text{silica}) \quad (\text{A3})$$

$$\mathbf{f} = -\frac{1}{2} \varepsilon_0 \gamma_e \nabla |\mathbf{E}|^2 \quad (\text{CS}_2). \quad (\text{A4})$$

In these expressions, we neglect the modal differences between the pump and the Stokes fields, the electrostrictive forces along the z-direction, and the radiation pressure.

Combining results for  $G_{B,j}$  with the complex eigenfrequencies, we can predict the spontaneous forward Brillouin scattering power spectrum using Eq. (1).

To obtain the complex acoustic eigenfrequencies for the LCOF system, we utilize a finite-element solver to numerically solve the damped wave equation for the elastic displacement  $\mathbf{u}$  where we assume stress free boundary conditions on the outside of the buffer. For the isotropic media that make up the LCOF, the elastic wave equation in the frequency domain is given by

$$-\rho \omega^2 \mathbf{u} = (1 - i/Q)(\mu \nabla^2 \mathbf{u} + (\lambda + \mu) \nabla \nabla \cdot \mathbf{u}) \quad (\text{A5})$$

where  $\lambda$  and  $\mu$  are the material specific Lamé parameters (in terms of longitudinal and shear sound speed  $v_L$  and  $v_T$  respectively,  $\lambda + 2\mu = \rho v_L^2$  and  $\mu = \rho v_T^2$ ) and  $Q$  is the frequency-dependent quality factor. In terms of elastic moduli given in Tab. I, Young's modulus is given by  $\mu(3\lambda + 2\mu)/(\lambda + \mu)$  and  $\mu$  is the shear modulus.

Acoustic dissipation critically determines the predicted power spectrum shown in Fig. 6. We account for dissipation by including empirically obtained frequency-dependent acoustic quality factors for silica and CS<sub>2</sub> in our simulations [23, 24]. In particular, we find that the polyimide buffer plays a crucial role in determining the power spectrum, similar to observations in early forward Brillouin scattering measurements [14]. We model acoustic absorption within the buffer by implementing a perfectly matched layer within the polyimide layer in addition to giving it a large constant acoustic damping ( $Q$ -factor 0.1).

material	parameter	value
CS <sub>2</sub>	density	1260 kg/m <sup>3</sup>
	refractive index	1.5885
	speed of sound	1242 m/s
	electrostrictive constant ( $\gamma_e$ )	2.279
SiO <sub>2</sub>	density	2203 kg/m <sup>3</sup>
	refractive index	1.445
	Young's modulus	73.1 GPa
	shear modulus	31.24 GPa
	phot. elas. tensor ( $p_{11}, p_{12}, p_{44}$ )	(0.125, 0.27, -0.073)
polyimide	density	1420 kg/m <sup>3</sup>
	Young's modulus	2.5 GPa
	shear modulus	0.933 GPa.

TABLE I. Simulation parameters used in simulations of spontaneous forward Brillouin scattering spectra.

[1] P. Dainese, P. S. J. Russell, G. S. Wiederhecker, N. Joly, H. L. Fragnito, V. Laude, and A. Khelif, *Optics express* **14**, 4141 (2006).  
[2] P. Dainese, P. S. J. Russell, N. Joly, J. Knight, G. Wiederhecker, H. L. Fragnito, V. Laude, and A. Khelif, *Nature Physics* **2**, 388 (2006).

[3] M. S. Kang, A. Nazarkin, A. Brenn, and P. S. J. Russell, *Nature Physics* **5**, 276 (2009).  
[4] H. Shin, W. Qiu, R. Jarecki, J. A. Cox, R. H. Olsson III, A. Starbuck, Z. Wang, and P. T. Rakich, *Nature communications* **4**, 1944 (2013).  
[5] J.-C. Beugnot, T. Sylvestre, H. Maillotte, G. Mélin, and

- V. Laude, Optics letters **32**, 17 (2007).
- [6] H. Shin, J. A. Cox, R. Jarecki, A. Starbuck, Z. Wang, and P. T. Rakich, Nature communications **6**, 6427 (2015).
- [7] M. S. Kang, A. Butsch, and P. S. J. Russell, Nature Photonics **5**, 549 (2011).
- [8] E. A. Kittlaus, H. Shin, and P. T. Rakich, Nature Photonics **10**, 463 (2015).
- [9] R. Van Laer, B. Kuyken, D. Van Thourhout, and R. Baets, Nature Photonics **9**, 199 (2015).
- [10] N. T. Otterstrom, E. A. Kittlaus, S. Gertler, R. O. Behunin, A. L. Lentine, and P. T. Rakich, arXiv:1903.03907.
- [11] N. T. Otterstrom, R. O. Behunin, E. A. Kittlaus, Z. Wang, and P. T. Rakich, Science **360**, 1113 (2018).
- [12] N. T. Otterstrom, R. O. Behunin, E. A. Kittlaus, and P. T. Rakich, Physical Review X **8**, 041034 (2018).
- [13] R. Shelby, M. Levenson, and P. Bayer, Physical review letters **54**, 939 (1985).
- [14] R. Shelby, M. Levenson, and P. Bayer, Physical Review B **31**, 5244 (1985).
- [15] K. Kieu, L. Schneebeli, R. A. Norwood, and N. Peyghambarian, Optics Express **20**, 8148 (2012).
- [16] K. Kieu, D. Churin, L. Schneebeli, R. A. Norwood, and N. Peyghambarian, Optics letters **38**, 543 (2013).
- [17] W. Qiu, P. T. Rakich, H. Shin, H. Dong, M. Soljačić, and Z. Wang, Optics express **21**, 31402 (2013).
- [18] W. H. Renninger, R. O. Behunin, and P. T. Rakich, Optica **3**, 1316 (2016).
- [19] W. H. Renninger, R. Behunin, and P. Rakich, in *CLEO: QELS\_Fundamental Science* (Optical Society of America, 2016) pp. FM4A–6.
- [20] P. Kharel, R. O. Behunin, W. H. Renninger, and P. T. Rakich, Physical Review A **93**, 063806 (2016).
- [21] R. W. Boyd, *Nonlinear Optics* (Academic press, 2003).
- [22] P. T. Rakich, C. Reinke, R. Camacho, P. Davids, and Z. Wang, Physical Review X **2**, 011008 (2012).
- [23] R. W. Coakley and R. W. Detenbeck, JOSA **65**, 6 (1975).
- [24] R. Vacher, J. Pelous, F. Plicque, and A. Zarembowitch, Journal of Non-Crystalline Solids **45**, 397 (1981).
- [25] J. Wang, Y. Zhu, R. Zhang, and D. J. Gauthier, Optics express **19**, 5339 (2011).
- [26] D. M. Chow, Z. Yang, M. A. Soto, and L. Thévenaz, Nature communications **9**, 2990 (2018).
- [27] Y. Antman, A. Clain, Y. London, and A. Zadok, Optica **3**, 510 (2016).